# JCAMECH

# A damage model incorporating dynamic plastic yield surface

## M. Ganjiani*

*Department of Mechanical Engineering, College of Engineering, University of Tehran, P.O. Box 11155-4563, Tehran, Iran*

## Abstract

In this paper, a general elastoplastic-damage constitutive model considering the effect of strain rate has been developed. The derivation of this model has been cast into the irreversible thermodynamics with internal variables within the fundamentals of Continuum Damage Mechanics (CDM). The rate effect has been involved as an additional term into the plastic yield surface (dynamic plastic yield surface). Therefore, the plastic surface has been presented in the category of Consistency–type model in which the rate of state variables is considered as independent state variables. The damage has been assumed as a tensor type variable and based on the energy equivalence hypothesis the damage evolution has been developed. The proposed model has been validated for both rate-independent and rate-dependent deformation. For this manner, the generalized trapezoidal stress integration algorithm of the model has been explained and the model has been implemented into user-defined subroutines (UMAT and VUMAT) in the finite element program ABAQUS. The results of numerical simulation, statically and dynamically, have been compared to the experimental results of three aluminum and two steel alloys. Also, the results of simulation for shear and double-notched tests have been compared to their experiments. By comparing the predicted results with experimental data, the capability and validity of the model have been verified.

## 1. Introduction

Plasticity theory itself cannot predict the softening effect in material behavior. Therefore, the theory of Continuum Damage Mechanics (CDM) has been coupled to the plasticity to describe this phenomenon. It is observed experimentally that the deformation response of material as well as damage evolution is influenced by strain-rate, temperature, history of loading, and stress [1-3]. The study of the dynamic deformation and fracture of materials by taking into account the damage evolution has become one of the research frontiers, receiving more and more attention by scientists until now [4-6].

For the analysis of many rate-dependent processes such as metal forming, impact, crash, and others, various viscoplastic models have been developed. Two types of modeling have been widely used in order to account the viscoplastic behavior of materials: the

---

* *Email Address*: ganjiani@ut.ac.ir, Tel: +98 21 82084858, Fax: +98 21 88013029

overstress (*Perzyna*)–type model [7, 8] and the *Consistency*–type model [9-14]. In the *Perzyna*–type model, a rate-independent yield function is used to describe the viscoplastic behavior of materials. The overstress effect in this model means that this yield function can become larger than zero. Using the overstress model, the consistency conditions are not fulfilled and the stress states outside the yield surface are allowed (c.f. [15]). The main problems of the overstress model have been discussed in Ref. [16]. In the *Consistency*–type model, the rates of state variables are considered as independent state variables and they are included in the yield function. Therefore, the time derivative of rate dependent yield function illustrates the viscoplastic behavior of materials.

Coupling a damage model with *Perzyna*–type approach is widely used in the literature to describe the rate-dependent (viscous) damage behavior [17-22]. Heeres et al. [12] compared the elastic-viscoplastic characteristics of the *Perzyna*– and *Consistency*–type models regarding the viscoplastic multiplier. In the *Perzyna*–type model, the rate of viscoplastic multiplier is explicitly defined via an overstress function, while in the *Consistency*–type model it is governed by a non-homogeneous differential equation. As they illustrated, the different responses during the stress reversals are the dissimilarities of these two models. Voyiadjis and Abed [23] proposed a coupled temperature and strain rate microstructure physically based yield function to derive a kinematical model for thermo-viscoplastic deformations of BCC metals. In their work, the viscoplastic multiplier is obtained using both the *Consistency*– and *Perzyna*–type viscoplasticity models and in the case of the *Perzyna* viscoplasticity model, the athermal yield function is employed instead of the static yield function.

The lack of research on developing a viscous damage model to be consistent with irreversible thermodynamics is obvious. In this analogy, Saksala et al. [14] developed a constitutive model by combining continuum damage with embedded discontinuity for dynamic analyses of quasi-brittle failure phenomena. Their model involves a rate-dependent continuum damage with isotropic hardening formulated in the *Consistency*–type approach.

The main objective of this paper is to propose a rate-dependent elastoplastic-damage model in the framework of continuum damage mechanics based on the *Consistency*–type approach. The effect of strain-rate is introduced by an additional term involved into the plastic yield surface. This implies that the proposed model is formulated in the *Consistency*–type approach. Appropriate thermodynamically consistent internal variables are identified. For numerical purposes, the generalized trapezoidal algorithm of the model is presented. In addition, in order to verify the capability of the model, the model is implemented as a user-defined subroutine UMAT/VUMAT in the finite element program ABAQUS and the simulation results are compared with the experiment data.

## 2. Constitutive model

### 2.1. *Thermodynamic conjugates*

In the concept of damage mechanics, the effective stress tensor $\boldsymbol{\sigma}$ is assumed to be:

$$\bar{\boldsymbol{\sigma}} = \mathbb{M}(\mathbf{D}):\boldsymbol{\sigma} \qquad (1)$$

where $\mathbb{M}(\mathbf{D})$ is a fourth-order symmetric tensor which denotes the damage effect tensor [24]. This tensor has the following form within the Voight notation:

$$\mathbb{M}(\mathbf{D}) = \text{diagonal}\left[\frac{1}{1-D_1} \quad \frac{1}{1-D_2} \quad \frac{1}{1-D_3} \quad \frac{1}{\sqrt{(1-D_2)(1-D_3)}} \quad \frac{1}{\sqrt{(1-D_3)(1-D_1)}} \quad \frac{1}{\sqrt{(1-D_1)(1-D_2)}}\right] (2)$$

where $D_1$, $.D_2$. and $D_3$ are principal values of damage tensor $\mathbf{D}$. Based on the rules of irreversible thermodynamics, the thermodynamic forces conjugated to the thermodynamic variables can be defined as:

$$\boldsymbol{\varepsilon}^e(\boldsymbol{\sigma},\mathbf{D}) = \mathbb{M}:\mathbb{C}_{e0}^{-1}:\mathbb{M}:\boldsymbol{\sigma} = \mathbb{C}_e^{-1}:\boldsymbol{\sigma}$$

$$\mathbf{Y}(\boldsymbol{\sigma},\mathbf{D}) = \boldsymbol{\sigma}^T:\mathbb{M}:\mathbb{C}_{e0}^{-1}:\frac{\partial\mathbb{M}(\mathbf{D})}{\partial\mathbf{D}}:\boldsymbol{\sigma} \qquad (3)$$

$$\sigma_h(r) = Kr^n$$

$$Y_h(\beta) = K_d\beta\exp(m_d\beta)$$

where $\mathbf{Y}$ is the damage energy release rate, $\sigma_h$

represents the isotropic hardening for plastic deformation and $Y_h$ is treated as isotropic hardening for damage evolution. $r$ is the effective plastic strain and $\beta$ is the accumulated damage. The sound elastic stiffness tensor, $\mathbb{C}_{e0}$, is considered as:

$$\mathbb{C}_{e0} = 2\mu\mathbb{I}^s + \lambda\mathbf{I}\otimes\mathbf{I} \quad , \quad (\mathbb{C}_{e0})_{ijkl} =$$

$$\mu(\delta_{ik}\delta_{jl} + \delta_{il}\delta_{jk}) + \lambda\delta_{ij}\delta_{kl} \qquad (4)$$

with $\mathbb{I}^s$ and $\mathbf{I}$ as the symmetric identity tensors of fourth- and second-order, and $\mu$, $\lambda$ as the *Lamé* constants which are related to Young's modulus $E$ and Poisson's ration $\upsilon$. Using the hypothesis of normal dissipation, the evolution equations of the

internal variables can be obtained as:

$$\dot{\boldsymbol{\varepsilon}}^{\mathrm{p}} = \dot{\zeta}^{\mathrm{p}} \frac{\partial f^{\mathrm{p}}}{\partial \boldsymbol{\sigma}} \quad , \quad \dot{r} = -\dot{\zeta}^{\mathrm{p}} \frac{\partial f^{\mathrm{p}}}{\partial \sigma_h} \quad ,$$

$$\dot{\mathbf{D}} = \dot{\zeta}^{\mathrm{d}} \frac{\partial f^{\mathrm{d}}}{\partial \mathbf{Y}} \quad , \quad \dot{\beta} = -\dot{\zeta}^{\mathrm{d}} \frac{\partial f^{\mathrm{d}}}{\partial Y_h} \tag{5}$$

where $f^{\mathrm{p}}$ and $f^{\mathrm{d}}$ are limiting functions which denote respectively the plastic and damage dissipation potentials (yield surfaces), and, $\dot{\zeta}^{\mathrm{p}}$ and $\dot{\zeta}^{\mathrm{d}}$ are two positive variables known as the plastic and damage multipliers.

### 2.2. Yield criteria

#### 2.2.1. Damage surface

The damage yield surface determines the possibility of damage propagation. The following relationship for the damage yield criterion is a modified version of [25] adopted in this paper:

$$f^{\mathrm{d}}\left(\mathbf{Y}, B; \mathbf{D}, \beta, r\right) = \|\mathbf{Y}\| - Y_0 - Y_h\left(\beta\right) =$$
$$\left(\frac{1}{2} \mathbf{Y}^T : \mathbf{L}(r) : \mathbf{Y}\right)^{1/2} - Y_0 - Y_h\left(\beta\right) \tag{6}$$

where $\mathbf{L}$ is a second-order positive damage characteristic tensor describing the damage induced change in the damage surface. The parameter $Y_0$ in equation (6) is a material constant used to specify the size of the initial damage surface. The evolution law for damage is characterized as:

$$\dot{\mathbf{D}} = \dot{\zeta}^{\mathrm{d}} \frac{\partial f^{\mathrm{d}}}{\partial \mathbf{Y}} = \dot{\zeta}^{\mathrm{d}} \mathbf{N}^{\mathrm{d}}$$
$$\dot{\beta} = -\dot{\zeta}^{\mathrm{d}} \frac{\partial f^{\mathrm{d}}}{\partial Y_h} = \dot{\zeta}^{\mathrm{d}} \tag{7}$$

In addition, the following Kuhn-Tucker relations control the damage evolution:

$$f^{\mathrm{d}} \leq 0 \quad , \quad \dot{\zeta}^{\mathrm{d}} \geq 0 \quad , \quad \dot{\zeta}^{\mathrm{d}} f^{\mathrm{d}} = 0 \tag{8}$$

The unit tensor $\mathbf{N}^{\mathrm{d}}$, which is normal to the damage surface, describes the direction of damage propagation as:

$$\mathbf{N}^{\mathrm{d}} = \frac{\mathbf{L} : \mathbf{Y}}{2\|\mathbf{Y}\|} \tag{9}$$

where $\mathbf{L}$ is the characteristic tensor defined here as:

$$\mathbf{L} = 2 \begin{bmatrix} 1 & \exp\left(-\eta_{\mathrm{d}} r\right) & \exp\left(-\eta_{\mathrm{d}} r\right) \\ & 1 & \exp\left(-\eta_{\mathrm{d}} r\right) \\ \text{sym s} & & 1 \end{bmatrix} \tag{10}$$

with $\eta_{\mathrm{d}}$ as a material constant which can be calibrated using experimental data.

#### 2.2.2. Plastic surface

The plastic yield criterion can be treated as a condition, which enables whether the plastic deformation occurs or only the elastic one happens. In this work, we developed a static/dynamic plastic yield function for rate-independent/dependent deformations, respectively. This yield criterion is defined as:

$$f^{\mathrm{p}}\left(\boldsymbol{\sigma}, R; \mathbf{D}, r\right) = \|\boldsymbol{\sigma}\| - \sigma_0 - \sigma_h\left(r, \dot{r}\right) =$$
$$\left(\frac{1}{2} \boldsymbol{\sigma}^T : \mathbb{M}^T\left(\mathbf{D}\right) : \mathbb{H} : \mathbb{M}\left(\mathbf{D}\right) : \boldsymbol{\sigma}\right)^{1/2} \tag{11}$$
$$-\sigma_0 - \sigma_h\left(r, \dot{r}\right)$$

where $\sigma_0$ is the initial strain hardening threshold and the positive definite tensor $\mathbb{H}$ for orthotropic materials is represented by a 6×6 matrix in the material principal coordinate system as:

$$\mathbb{H} = \begin{bmatrix} 2 & -1 & -1 & 0 & 0 & 0 \\ & 2 & -1 & 0 & 0 & 0 \\ & & 2 & 0 & 0 & 0 \\ & & & 6 & 0 & 0 \\ & & & & 6 & 0 \\ \text{sym s} & & & & & 6 \end{bmatrix} \tag{12}$$

The dependency of plastic yield function on the strain rate has been involved by the term $\sigma_h\left(r, \dot{r}\right)$ in equation (11). For the rate-independent plasticity, the term $\sigma_h\left(r, \dot{r}\right)$ is reduced to $\sigma_h\left(r\right)$ as referred in equation (3)₃. In rate-dependent plasticity concept, the behavior of BCC and FCC type materials is different. Therefore, the form of term $\sigma_h\left(r, \dot{r}\right)$ is different for FCC and BCC materials [26-28]. Here, we adopted $\sigma_h\left(r, \dot{r}\right)$ as:

$$\sigma_{hBBC}\left(r, \dot{r}\right) = \sigma_0\left(\dot{r}/\dot{r}_0\right)^c + \sigma_h\left(r\right)$$
$$\sigma_{hFCC}\left(r, \dot{r}\right) = \left(\sigma_0 + \sigma_h\left(r\right)\right)\left(\dot{r}/\dot{r}_0\right)^c \tag{13}$$

where $\dot{r}$ is the plastic strain-rate, $\dot{r}_0$ is a lower bound

strain-rate and $_c$ is the strain-rate sensitivity parameter. Substituting yield function (11) into (5) yields the plastic strain increment $\dot{\boldsymbol{\varepsilon}}^{\mathrm{p}}$ and the increment of isotropic hardening variable $\dot{r}$ as follows:

$$
\dot{\boldsymbol{\varepsilon}}^{\mathrm{p}} = \dot{\zeta}^{\mathrm{p}} \frac{\partial f^{\mathrm{p}}}{\partial \boldsymbol{\sigma}} = \dot{\zeta}^{\mathrm{p}} \mathbf{N}^{\mathrm{p}}
$$

$$
\dot{r} = -\dot{\zeta}^{\mathrm{p}} \frac{\partial f^{\mathrm{p}}}{\partial \sigma_h} = \dot{\zeta}^{\mathrm{p}} \tag{14}
$$

where the second-order tensor $\mathbf{N}^{\mathrm{p}}$ is the normal direction to the plastic yield surface:

$$
\mathbf{N}^{\mathrm{p}} = \frac{\mathbb{M}^{T} : \mathbb{H} : \mathbb{M} : \boldsymbol{\sigma}}{2\|\boldsymbol{\sigma}\|} \tag{15}
$$

The plastic yield surface, equation (11), should also satisfy the following Kuhn-Tucker loading/unloading conditions:

$$
f^{\mathrm{p}} \leq 0 \;,\;\; \dot{\zeta}^{\mathrm{p}} \geq 0 \;,\;\; \dot{\zeta}^{\mathrm{p}} f^{\mathrm{p}} = 0 \tag{16}
$$

## 3. Stress update algorithm

The constitutive equations described in the previous sections are summarized as:

$$
\begin{aligned}
\dot{\boldsymbol{\sigma}} &= \mathbb{C}_{\mathrm{e}} : \dot{\boldsymbol{\varepsilon}}^{\mathrm{e}} \\
\dot{\boldsymbol{\varepsilon}}^{\mathrm{p}} &= \dot{\zeta}^{\mathrm{p}} \mathbf{N}^{\mathrm{p}} \\
\dot{\mathbf{D}} &= \dot{\zeta}^{\mathrm{d}} \mathbf{N}^{\mathrm{d}} \\
\dot{r} &= \dot{\zeta}^{\mathrm{p}} \\
\dot{\beta} &= \dot{\zeta}^{\mathrm{d}}
\end{aligned}
$$

$$
\dot{f}^{\mathrm{p}}(\boldsymbol{\sigma}, R; \mathbf{D}, r, \dot{r}) \;\; \begin{aligned} f^{\mathrm{p}}_{,\boldsymbol{\sigma}} : \dot{\boldsymbol{\sigma}} + f^{\mathrm{p}}_{,\mathbf{D}} : \dot{\mathbf{D}} + \\ f^{\mathrm{p}}_{,r} \dot{r} + f^{\mathrm{p}}_{,\dot{r}} \ddot{r} \end{aligned} = 0
$$

$$
\dot{f}^{\mathrm{d}}(\mathbf{Y}, B; \mathbf{D}, \beta, r) \;\; \begin{aligned} = f^{\mathrm{d}}_{,\boldsymbol{\sigma}} : \dot{\boldsymbol{\sigma}} + f^{\mathrm{d}}_{,\mathbf{D}} : \dot{\mathbf{D}} + \\ f^{\mathrm{d}}_{,\beta} \dot{\beta} + f^{\mathrm{d}}_{,r} \dot{r} \end{aligned} = 0 \tag{17}
$$

The aim of integration algorithm is that using the input data $\{\boldsymbol{\varepsilon}_n, \boldsymbol{\varepsilon}^{\mathrm{p}}_n, \boldsymbol{\sigma}_n, \mathbf{D}_n, r_n, \dot{r}_n, \beta_n\}$ at time $t_n$ and applying the strain increment $\Delta\boldsymbol{\varepsilon}$, the variables $\{\boldsymbol{\varepsilon}_{n+1}, \boldsymbol{\varepsilon}^{\mathrm{p}}_{n+1}, \boldsymbol{\sigma}_{n+1}, \mathbf{D}_{n+1}, r_{n+1}, \dot{r}_{n+1}, \beta_{n+1}\}$ are obtained by satisfying the loading-unloading

conditions at time $t_{n+1}$. In what follows, we represent the generalized trapezoidal scheme algorithm of the proposed model.

### 3.1. *Generalized trapezoidal scheme*

The proposed constitutive equations are integrated using a *generalized trapezoidal integration algorithm*. At this algorithm, the plastic strain increment and the increment of internal variables are calculated at the end time, i.e., $t_{n+1}$. During this calculation, the satisfaction of either/both plastic and damage surfaces is established. Therefore, the integration algorithm is written as:

$$
\begin{aligned}
\boldsymbol{\varepsilon}_{n+1} &= \boldsymbol{\varepsilon}_n + \Delta\boldsymbol{\varepsilon} \\
\boldsymbol{\varepsilon}^{\mathrm{p}}_{n+1} &= \boldsymbol{\varepsilon}^{\mathrm{p}}_n + \Delta\zeta^{\mathrm{p}}_{n+1} \mathbf{N}^{\mathrm{p}}_{n+\theta} \\
\mathbf{D}_{n+1} &= \mathbf{D}_n + \Delta\zeta^{\mathrm{d}}_{n+1} \mathbf{N}^{\mathrm{d}}_{n+\theta} \\
r_{n+1} &= r_n + \Delta\zeta^{\mathrm{p}}_{n+1} \\
\dot{r}_{n+1} &= \Delta\zeta^{\mathrm{p}}_{n+1} / \Delta t \\
\beta_{n+1} &= \beta_n + \Delta\zeta^{\mathrm{d}}_{n+1} \\
\boldsymbol{\sigma}_{n+1} &= \mathbb{C}_{\mathrm{e}}(\mathbf{D}_{n+1}) : (\boldsymbol{\varepsilon}_{n+1} - \boldsymbol{\varepsilon}^{\mathrm{p}}_{n+1}) \\
f^{\mathrm{p}}_{n+1}(\boldsymbol{\sigma}_{n+1}, \mathbf{D}_{n+1}, r_{n+1}, \dot{r}_{n+1}) &= 0 \\
f^{\mathrm{d}}_{n+1}(\mathbf{Y}_{n+1}, \mathbf{D}_{n+1}, \beta_{n+1}, r_{n+1}) &= 0
\end{aligned} \tag{18}
$$

where by $0 \leq \theta \leq 1$, the normal directions to the plastic and damage surfaces are determined as a weighted average of them at the beginning and end of the step: $\mathbf{N}_{n+\theta} = (1-\theta)\mathbf{N}_n + \theta\mathbf{N}_{n+1}$. Clearly, the fully explicit Euler forward method is retrieved when $\theta = 0$, while the implicit Euler backward method is obtained for $\theta = 1$. The nonlinear equations of (18) are solved for the parameters with subscript $n+1$. The equation $(18)_2$ can be rewritten in the following form:

$$
\Delta\boldsymbol{\varepsilon}^{\mathrm{p}}_{n+1} \equiv \boldsymbol{\varepsilon}^{\mathrm{p}}_{n+1} - \boldsymbol{\varepsilon}^{\mathrm{p}}_n = \Delta\zeta^{\mathrm{p}}_{n+1} \mathbf{N}^{\mathrm{p}}_{n+\theta} \tag{19}
$$

Substituting this equation into $(18)_7$, we will have:

$$
\boldsymbol{\sigma}_{n+1} = \mathbb{C}_{\mathrm{e}}(\mathbf{D}_{n+1}) : \left(\boldsymbol{\varepsilon}^{\mathrm{e}}_n + \Delta\boldsymbol{\varepsilon} - \Delta\boldsymbol{\varepsilon}^{\mathrm{p}}_{n+1}\right) \tag{20}
$$

If we write $\mathbb{C}_{\mathrm{e}}(\mathbf{D}_{n+1})$ as $\mathbb{C}_{\mathrm{e}(n+1)}$, equation (20) is simplified to:

$$
\mathbb{C}^{-1}_{\mathrm{e}(n+1)} : \boldsymbol{\sigma}_{n+1} = \boldsymbol{\varepsilon}^{\mathrm{e}}_n + \Delta\boldsymbol{\varepsilon} - \Delta\boldsymbol{\varepsilon}^{\mathrm{p}}_{n+1} \tag{21}
$$

Double contracting both sides of equation (21) at

$\mathbb{C}_{\mathrm{e}(n)}$ yields:

$$\mathbb{C}_{\mathrm{e}(n)} : \mathbb{C}_{\mathrm{e}(n+1)}^{-1} : \boldsymbol{\sigma}_{n+1} = \boldsymbol{\sigma}_{n+1}^{\mathrm{trial}} - \mathbb{C}_{\mathrm{e}(n)} : \Delta\boldsymbol{\varepsilon}_{n+1}^{\mathrm{p}} \quad (22)$$

where $\boldsymbol{\sigma}_{n+1}^{\mathrm{trial}} = \boldsymbol{\sigma}_n + \mathbb{C}_{\mathrm{e}(n)} : \Delta\boldsymbol{\varepsilon}$ is the trial stress. In the integration of the model, a return-mapping algorithm involving the elastic predictor and plastic/damage corrector is used. During the plastic/damage corrector, the total strain is constant and linearization is established based on the increment of $\Delta\zeta^{\mathrm{p}}$ and $\Delta\zeta^{\mathrm{d}}$.

### 3.1.1. *Linearization*

Subsequently, we neglect the subscript $n+1$ for simplicity. The equations (18) are as consistent with the Newton-Raphson method:

$$f^{\mathrm{p}(k)} + \left(\frac{\partial f^{\mathrm{p}}}{\partial \boldsymbol{\sigma}}\right)^{(k)} : \Delta\boldsymbol{\sigma}^{(k)} + \left(\frac{\partial f^{\mathrm{p}}}{\partial \mathbf{D}}\right)^{(k)} : \Delta\mathbf{D}^{(k)} + \left(\frac{\partial f^{\mathrm{p}}}{\partial \Delta\zeta^{\mathrm{p}}} + \frac{1}{\Delta t}\frac{\partial f^{\mathrm{p}}}{\partial \Delta\dot{\zeta}^{\mathrm{p}}}\right)^{(k)} \delta\zeta^{\mathrm{p}(k)} = 0$$

$$f^{\mathrm{d}(k)} + \left(\frac{\partial f^{\mathrm{d}}}{\partial \boldsymbol{\sigma}}\right)^{(k)} : \Delta\boldsymbol{\sigma}^{(k)} + \left(\frac{\partial f^{\mathrm{d}}}{\partial \mathbf{D}}\right)^{(k)} : \Delta\mathbf{D}^{(k)} + \left(\frac{\partial f^{\mathrm{d}}}{\partial \Delta\zeta^{\mathrm{d}}}\right)^{(k)} \delta\zeta^{\mathrm{d}(k)} + \left(\frac{\partial f^{\mathrm{d}}}{\partial \Delta\zeta^{\mathrm{p}}}\right)^{(k)} \delta\zeta^{\mathrm{p}(k)} = 0$$

$$(25)$$

where $\partial f^{\mathrm{p}} / \partial \Delta\zeta^{\mathrm{d}} = 0$ is exploited in equation

$$\frac{\partial \mathbf{r}_{\boldsymbol{\sigma}}}{\partial \boldsymbol{\sigma}} = \mathbb{C}_{\mathrm{e}}^{-1} + \Delta\zeta^{\mathrm{p}}\mathbf{N}_{n+\theta,\boldsymbol{\sigma}}^{\mathrm{p}}$$

$$\frac{\partial \mathbf{r}_{\boldsymbol{\sigma}}}{\partial \mathbf{D}} = \mathbb{C}_{\mathrm{e},\mathbf{D}}^{-1} : \boldsymbol{\sigma} + \Delta\zeta^{\mathrm{p}}\mathbf{N}_{n+\theta,\mathbf{D}}^{\mathrm{p}}$$

$$\frac{\partial \mathbf{r}_{\boldsymbol{\sigma}}}{\partial \Delta\zeta^{\mathrm{p}}} = \mathbf{N}_{n+\theta}^{\mathrm{p}}$$

$$\frac{\partial \mathbf{r}_{\boldsymbol{\sigma}}}{\partial \Delta\zeta^{\mathrm{d}}} = \mathbf{0}$$

In what follows, we write all equations in the matrix-vector format. Substituting equations (26) into (24), the resultant equations can be written in the matrix form as:

in numerical algorithm. Focusing on equations (24), the partial derivatives observed in these two equations

$$\mathbf{r}_{\boldsymbol{\sigma}} = \mathbb{C}_{\mathrm{e}}^{-1} : \boldsymbol{\sigma} - \mathbb{C}_{\mathrm{e}(n)}^{-1} : \boldsymbol{\sigma}_{n+1}^{\mathrm{trial}} + \Delta\zeta^{\mathrm{p}}\mathbf{N}_{n+\theta}^{\mathrm{p}}$$

$$\mathbf{r}_{\mathbf{D}} = -\mathbf{D} + \mathbf{D}_n + \Delta\zeta^{\mathrm{d}}\mathbf{N}_{n+\theta}^{\mathrm{d}}$$

$$f^{\mathrm{p}} = f^{\mathrm{p}}\left(\boldsymbol{\sigma}, \mathbf{D}, r, \dot{r}\right)$$

$$f^{\mathrm{d}} = f^{\mathrm{d}}\left(\mathbf{Y}, \mathbf{D}, \beta, r\right)$$

$$(23)$$

Linearizing equations (23) yields

$$\mathbf{r}_{\boldsymbol{\sigma}}^{(k)} + \left(\frac{\partial \mathbf{r}_{\boldsymbol{\sigma}}}{\partial \boldsymbol{\sigma}}\right)^{(k)} : \Delta\boldsymbol{\sigma}^{(k)} + \left(\frac{\partial \mathbf{r}_{\boldsymbol{\sigma}}}{\partial \mathbf{D}}\right)^{(k)} : \Delta\mathbf{D}^{(k)} + \left(\frac{\partial \mathbf{r}_{\boldsymbol{\sigma}}}{\partial \Delta\zeta^{\mathrm{p}}}\right)^{(k)} \delta\zeta^{\mathrm{p}(k)} + \left(\frac{\partial \mathbf{r}_{\boldsymbol{\sigma}}}{\partial \Delta\zeta^{\mathrm{d}}}\right)^{(k)} \delta\zeta^{\mathrm{d}(k)} = 0$$

$$\mathbf{r}_{\mathbf{D}}^{(k)} + \left(\frac{\partial \mathbf{r}_{\mathbf{D}}}{\partial \boldsymbol{\sigma}}\right)^{(k)} : \Delta\boldsymbol{\sigma}^{(k)} + \left(\frac{\partial \mathbf{r}_{\mathbf{D}}}{\partial \mathbf{D}}\right)^{(k)} : \Delta\mathbf{D}^{(k)} + \left(\frac{\partial \mathbf{r}_{\mathbf{D}}}{\partial \Delta\zeta^{\mathrm{p}}}\right)^{(k)} \delta\zeta^{\mathrm{p}(k)} + \left(\frac{\partial \mathbf{r}_{\mathbf{D}}}{\partial \Delta\zeta^{\mathrm{d}}}\right)^{(k)} \delta\zeta^{\mathrm{d}(k)} = 0$$

$$(24)$$

(25). The superscript $k$ denotes the iteration counter

$$\frac{\partial \mathbf{r}_{\mathbf{D}}}{\partial \boldsymbol{\sigma}} = \Delta\zeta^{\mathrm{d}}\mathbf{N}_{n+\theta,\boldsymbol{\sigma}}^{\mathrm{d}}$$

$$\frac{\partial \mathbf{r}_{\mathbf{D}}}{\partial \mathbf{D}} = -\mathbf{I} + \Delta\zeta^{\mathrm{d}}\mathbf{N}_{n+\theta,\mathbf{D}}^{\mathrm{d}}$$

$$\frac{\partial \mathbf{r}_{\mathbf{D}}}{\partial \Delta\zeta^{\mathrm{p}}} = \Delta\zeta^{\mathrm{d}}\mathbf{N}_{n+\theta,\Delta\zeta_{\mathrm{p}}}^{\mathrm{d}}$$

$$\frac{\partial \mathbf{r}_{\mathbf{D}}}{\partial \Delta\zeta^{\mathrm{d}}} = \mathbf{N}_{n+\theta}^{\mathrm{d}}$$

$$(26)$$

are obtained as:

$$\left[\mathbf{A}^{(k)}\right]^{-1} \left\{ \begin{array}{c} \Delta\boldsymbol{\sigma}^{(k)} \\ \Delta\mathbf{D}^{(k)} \end{array} \right\} = -\left\{\mathbf{r}^{(k)}\right\} - \left[\mathbf{N}^{(k)}\right]\left\{\delta\zeta^{(k)}\right\} \quad (27)$$

where

$$\left[\mathbf{A}^{(k)}\right]^{-1} = \begin{bmatrix} \mathbb{C}_e^{-1}+\Delta\zeta^p\mathbf{N}_{n+\theta,\boldsymbol{\sigma}}^p & \mathbb{C}_{e,\mathbf{D}}^{-1}:\boldsymbol{\sigma}+\Delta\zeta^p\mathbf{N}_{n+\theta,\mathbf{D}}^p \\ \Delta\zeta^d\mathbf{N}_{n+\theta,\boldsymbol{\sigma}}^d & -\mathbf{I}+\Delta\zeta^d\mathbf{N}_{n+\theta,\mathbf{D}}^d \end{bmatrix}^{(k)}, \quad \left[\mathbf{N}^{(k)}\right] = \begin{bmatrix} \mathbf{N}_{n+\theta}^p & \mathbf{0} \\ \Delta\zeta^d\mathbf{N}_{n+\theta,\Delta\zeta_p}^d & \mathbf{N}_{n+\theta}^d \end{bmatrix}^{(k)}$$

$$\left\{\mathbf{r}^{(k)}\right\} = \begin{Bmatrix} \mathbf{r}_{\boldsymbol{\sigma}}^{(k)} \\ \mathbf{r}_{\mathbf{D}}^{(k)} \end{Bmatrix}, \quad \left\{\delta\zeta^{(k)}\right\} = \begin{Bmatrix} \delta\zeta^{p(k)} \\ \delta\zeta^{d(k)} \end{Bmatrix}$$

$$(28)$$

Solving equation (27) for the increments of stress and damage gives:

$$\begin{Bmatrix} \Delta\boldsymbol{\sigma}^{(k)} \\ \Delta\mathbf{D}^{(k)} \end{Bmatrix} = -\left[\mathbf{A}^{(k)}\right]\left\{\mathbf{r}^{(k)}\right\} - \left[\mathbf{A}^{(k)}\right]\left[\mathbf{N}^{(k)}\right]\left\{\delta\zeta^{(k)}\right\} \quad (29)$$

Also, equations (25) in the matrix format yields:

$$\left\{f^{(k)}\right\} = \begin{Bmatrix} f^{p(k)} \\ f^{d(k)} \end{Bmatrix}, \quad \left[f_{\boldsymbol{\sigma}\mathbf{D}}^{(k)}\right] = \begin{bmatrix} f_{,\boldsymbol{\sigma}}^{p(k)} & f_{,\mathbf{D}}^{p(k)} \\ f_{,\boldsymbol{\sigma}}^{d(k)} & f_{,\mathbf{D}}^{d(k)} \end{bmatrix}, \quad \left[f_{\Delta\zeta}^{(k)}\right] = \begin{bmatrix} f_{,\Delta\zeta_p}^{p(k)}+\frac{1}{\Delta t}f_{,\Delta\dot\zeta_p}^{p(k)} & 0 \\ f_{,\Delta\zeta_p}^{d(k)} & f_{,\Delta\zeta_d}^{d(k)} \end{bmatrix} \quad (31)$$

So by substituting equation (29) into (30), and

$$\left\{f^{(k)}\right\} + \left[f_{\boldsymbol{\sigma}\mathbf{D}}^{(k)}\right]\begin{Bmatrix} \Delta\boldsymbol{\sigma}^{(k)} \\ \Delta\mathbf{D}^{(k)} \end{Bmatrix} + \left[f_{\Delta\zeta}^{(k)}\right]\left\{\delta\zeta^{(k)}\right\} = 0 \quad (30)$$

where

solving that for $\left\{\delta\zeta^{(k)}\right\}$ we will have:

$$\left\{\delta\zeta^{(k)}\right\} = \left[f_{\boldsymbol{\sigma}\mathbf{D}}^{(k)}\mathbf{A}^{(k)}\mathbf{N}^{(k)} - f_{\Delta\zeta}^{(k)}\right]^{-1}\left\{f^{(k)} - f_{\boldsymbol{\sigma}\mathbf{D}}^{(k)}\mathbf{A}^{(k)}\mathbf{r}^{(k)}\right\} \quad (32)$$

Now, as the $\left\{\delta\zeta^{(k)}\right\}$ was calculated, the values of $\left\{\Delta\boldsymbol{\sigma}^{(k)}\ \Delta\mathbf{D}^{(k)}\right\}$ can be obtained from equation (29).

Therefore, other internal variables are updated at the end of time step as follows:

$$\begin{aligned} \boldsymbol{\sigma}^{(k+1)} &= \boldsymbol{\sigma}^{(k)}+\Delta\boldsymbol{\sigma}^{(k)}, & r^{(k+1)} &= r^{(k)}+\delta\zeta^{p(k)}, & \Delta\zeta^{p(k+1)} &= \Delta\zeta^{p(k)}+\delta\zeta^{p(k)}, \\ \boldsymbol{\varepsilon}^{p(k+1)} &= \boldsymbol{\varepsilon}^{p(k)}+\Delta\boldsymbol{\varepsilon}^{p(k)}, & \dot r^{(k+1)} &= \dot r^{(k)}+\frac{1}{\Delta t}\delta\zeta^{p(k)}, & \Delta\zeta^{d(k+1)} &= \Delta\zeta^{d(k)}+\delta\zeta^{d(k)}, \\ \mathbf{D}^{(k+1)} &= \mathbf{D}^{(k)}+\Delta\mathbf{D}^{(k)}, & \beta^{(k+1)} &= \beta^{(k)}+\delta\zeta^{d(k)}. \end{aligned} \quad (33)$$

The iterations are repeated until the criterion $\text{norm}\left\{f^{(k+1)}\right\} < tol$ is established.

### 3.1.2. *The algorithmic tangent modulus*

In the implicit numerical methods, a suitable tangent modulus of the proposed algorithm is required for the fast convergent. This modulus is defined as:

$$\mathbb{C}^{alg} = \left(\frac{d\boldsymbol{\sigma}}{d\boldsymbol{\varepsilon}}\right)_{n+1} \quad (34)$$

For obtaining an expression for the tangent modulus, the increment form of equations (18) at time $t_{n+1}$ will be:

$$\begin{aligned} d\mathbb{C}_e^{-1}:\boldsymbol{\sigma}+\mathbb{C}_e^{-1}:d\boldsymbol{\sigma} &= d\boldsymbol{\varepsilon}-d\boldsymbol{\varepsilon}^p \\ d\boldsymbol{\varepsilon}^p &= d(\Delta\zeta^p)\mathbf{N}_{n+\theta}^p+\Delta\zeta^p d\mathbf{N}_{n+\theta}^p \\ d\mathbf{D} &= d(\Delta\zeta^d)\mathbf{N}_{n+\theta}^d+\Delta\zeta^d d\mathbf{N}_{n+\theta}^d \\ df^p &= f_{,\boldsymbol{\sigma}}^p:d\boldsymbol{\sigma}+f_{,\mathbf{D}}^p:d\mathbf{D}+\left\{f_{,\Delta\zeta_p}^p+\frac{1}{\Delta t}f_{,\Delta\dot\zeta_p}^p\right\}d(\Delta\zeta^p)+f_{,\Delta\zeta_d}^p d(\Delta\zeta^d) = 0 \\ df^d &= f_{,\boldsymbol{\sigma}}^d:d\boldsymbol{\sigma}+f_{,\mathbf{D}}^d:d\mathbf{D}+f_{,\Delta\zeta_p}^d d(\Delta\zeta^p)+f_{,\Delta\zeta_d}^d d(\Delta\zeta^d) = 0 \end{aligned} \quad (35)$$

16

By substituting (35)$_2$ into (35)$_1$ and employing (35)$_3$, we arrive at:

$$\left\{\begin{matrix} d\boldsymbol{\sigma} \\ d\mathbf{D} \end{matrix}\right\} = -[\mathbf{A}]\left\{\begin{matrix} d\boldsymbol{\varepsilon} \\ \mathbf{0} \end{matrix}\right\} - [\mathbf{A}][\mathbf{N}]\{d(\Delta\zeta)\} \quad (36)$$

In addition, by replacing equation (36) into (35)$_4$ and (35)$_5$, and solving them for $d(\Delta\zeta^{\mathrm{p}})$ and $d(\Delta\zeta^{\mathrm{d}})$, we get:

$$\left\{\begin{matrix} d(\Delta\zeta^{\mathrm{p}}) \\ d(\Delta\zeta^{\mathrm{d}}) \end{matrix}\right\} = \left[ f_{\Delta\zeta} - f_{\boldsymbol{\sigma}\mathbf{D}}\mathbf{A}\mathbf{N} \right]^{-1} \left\{ -f_{\boldsymbol{\sigma}\mathbf{D}}\mathbf{A} \right\} \left\{\begin{matrix} d\boldsymbol{\varepsilon} \\ \mathbf{0} \end{matrix}\right\} \quad (37)$$

By substituting this result into (36) we have:

$$\left\{\begin{matrix} d\boldsymbol{\sigma} \\ d\mathbf{D} \end{matrix}\right\} = \left[ \mathbf{A} - \mathbf{A}\mathbf{N}\otimes\left[ f_{\Delta\zeta} - f_{\boldsymbol{\sigma}\mathbf{D}}\mathbf{A}\mathbf{N} \right]^{-1}\left[ f_{\boldsymbol{\sigma}\mathbf{D}}\mathbf{A} \right]\right]\left\{\begin{matrix} d\boldsymbol{\varepsilon} \\ \mathbf{0} \end{matrix}\right\} \quad (38)$$

Equation (38), in fact, represents a relationship for algorithm tangent modulus of stress and damage tensors. The algorithm tangent modulus defined in (34) can be simply extracted from equation (38).

## 4. Model validation

### 4.1. *Rate-independent plasticity*

The rate-independent form of the proposed model is achieved when the coefficient $(\dot{r}/\dot{r}_0)^C$ in the plastic yield surface is omitted. This purpose can be fulfilled by putting $C$ as zero. In order to show the capability of the proposed model, the results of numerical simulation are compared to some published experimental data. The experimental results of three

aluminum and two steel alloys are chosen for this comparison. The material parameters of these materials are presented in Table . Only aluminum Al2024-T3 [29, 30] has data for $D_2$ and $D_1$, so the parameter $\eta_{\mathrm{d}}$ can be calculated only for this material. Fig. 1 shows the comparison of the numerical results with those experiments in stress and damage data for these materials. Fig. 1 shows that the damage variation may be different by the materials. These differences are specifically noticeable in the damage-strain curves. This model has properly predicted the stress-strain as well as the damage-strain curves of different materials. Based on Fig. 1, there are good agreements between simulation results and experimental data in both stress and damage data.

Table 1. The material parameters used in the model.

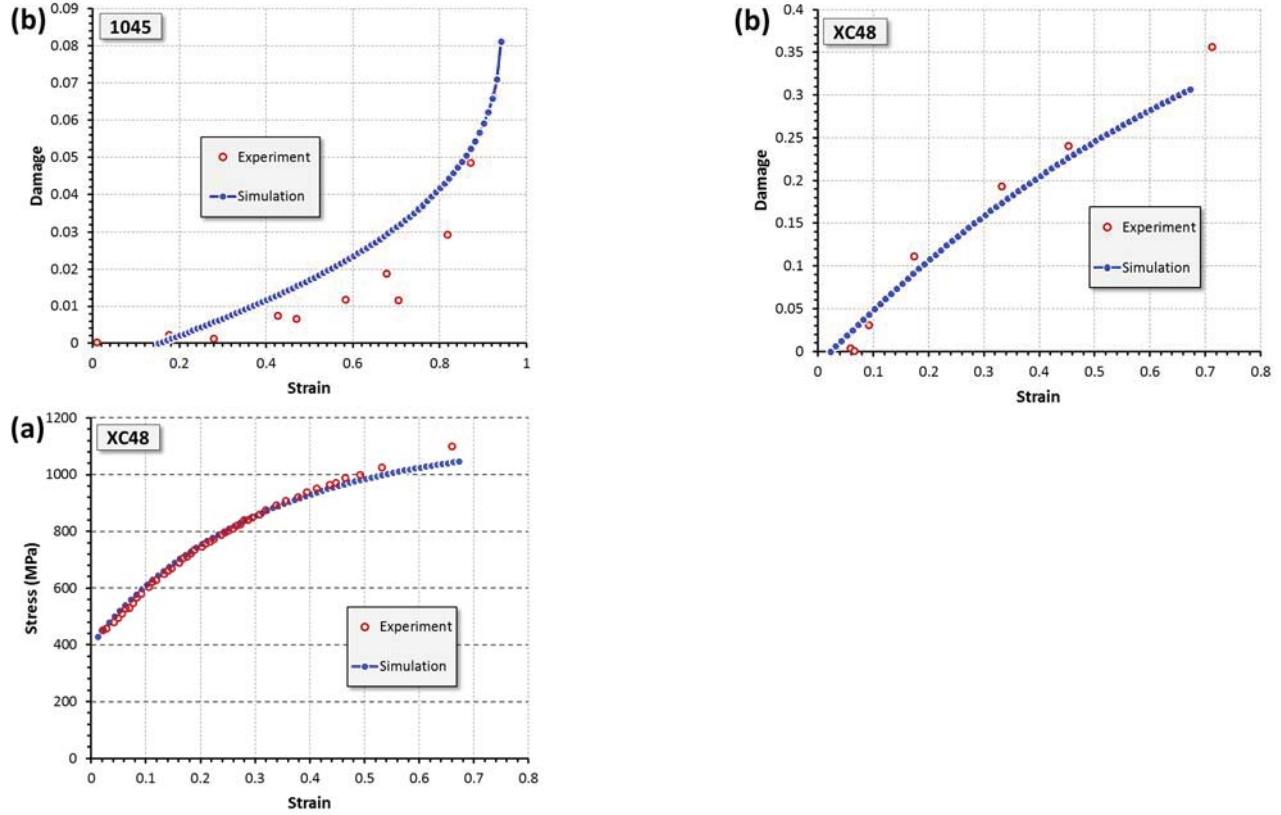| | $\upsilon$ | $E$ (GPa) | $\sigma_0$ (MPa) | $K$ (MPa) | $n$ | $Y_0$ (MPa) | $K_{\mathrm{d}}$ (MPa) | $m_{\mathrm{d}}$ | $\eta_{\mathrm{d}}$ | $c$ |
|---|---|---|---|---|---|---|---|---|---|---|
| Al2024-T3 [30] | 353 | 70 | 325 | 950 | 0.68 | 1.42 | 14.5 | 2.5 | 3.13 | 0.0053 |
| Al2024-T3 [29] | 0.33 | 74.5 | 345 | 1200 | 0.7 | 1.51 | 45 | 4.5 | 13.2 | — |
| A2017 [31] | 0.33 | 72.4 | 270 | 1200 | 0.7 | 0.65 | 30 | 0.5 | — | — |
| Steel 1045 [32] | 0.3 | 200 | 302 | 750 | 0.55 | 1.81 | 138 | -12 | — | 0.06 |
| Steel XC48 [31] | 0.3 | 200 | 400 | 2300 | 0.95 | 1.04 | 20 | 3 | — | — |
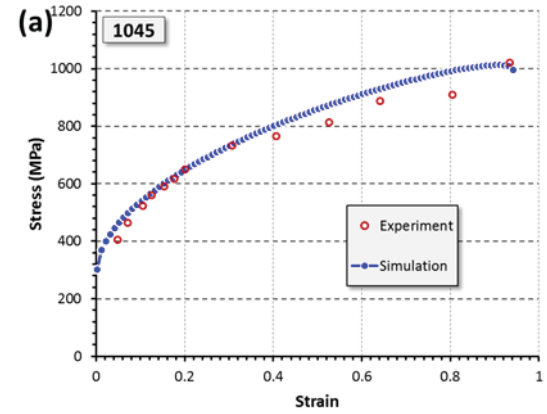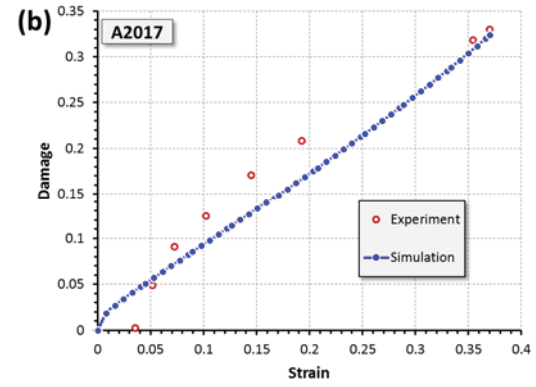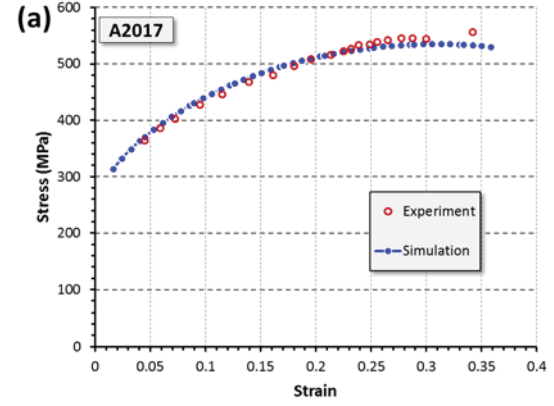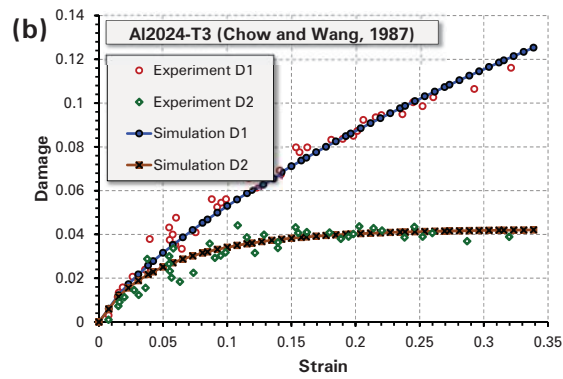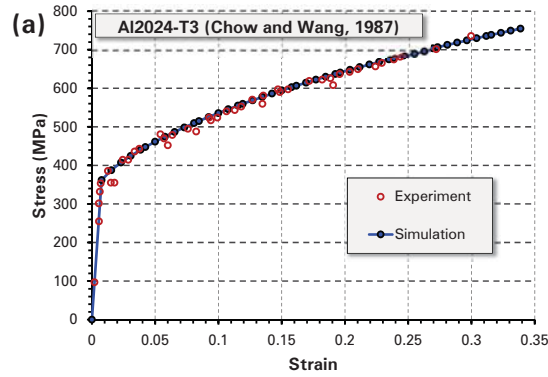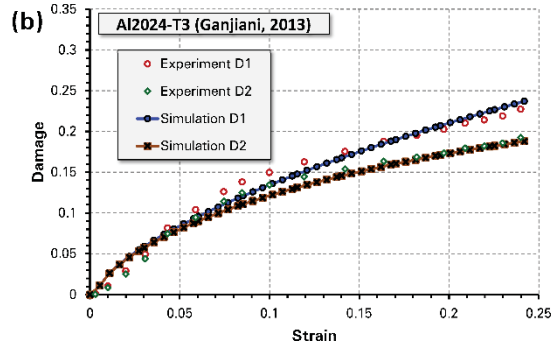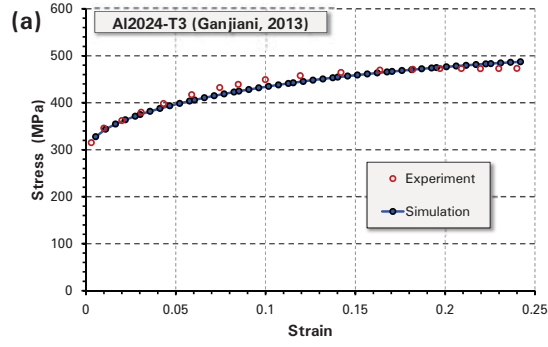
Fig. 1. (Continued) Comparison between the predicted results with experimental data via (a) stress-strain and (b) damage-strain curves for aluminum 2024-T3 [29, 30], aluminum A2017 [31], steel 1045 [32] and steelXC48 [31].

The shear test was conducted to verify the results of numerical simulation. The material used was aluminum alloy, 2024-T3 [30]. The shear specimen was designed based on the standard ASTM B831-93 shown in Fig. 2 with 3.2 mm thickness. The specimen was stretched with the velocity of 5 mm/min so that the tests can be considered as quasi-static.
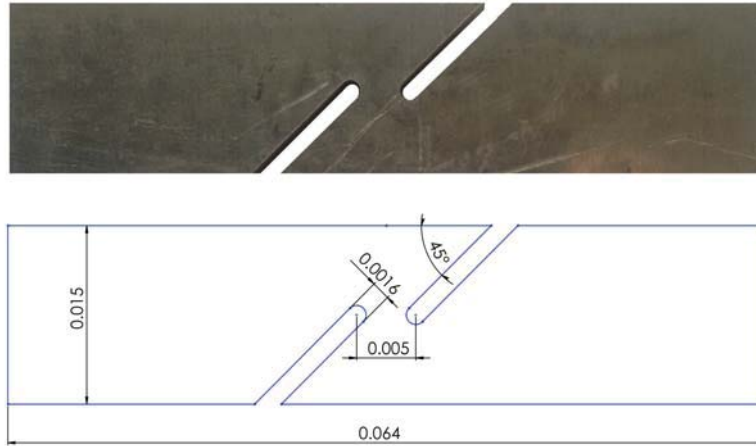


Fig. 2. The specimen of shear test (dimensions are in millimeter).

The results of shear test were compared numerically with experiment. Therefore, the model was implemented as a user-defined subroutine UMAT in the ABAQUS/Standard finite element program. The distribution of von-Mises stress, effective plastic strain and accumulated damage as well as a view of fracture specimen are shown in Fig. 3. These curves show that where the maximum plastic strains occur, the

accumulated damage has also maximum value. From this, it can be inferred that the damage may be related to the plastic strain.

Furthermore, for investigating the capability of model and validating the results, the predicted numerically load-displacement curve is shown in Fig. 4. The load at any time is calculated by summing nodes loads in a cross section far from the shear region. The figure shows a satisfactory agreement between experimental and numerical data.

### 4.1.1. *Rate-dependent plasticity*

The simulation results on steel 1045 as a BCC material are compared with experiments in uniaxial tensile/compressive tests. Fig. 5a shows the results of stress-strain curve in two different strain rates. At low strain rate (quasi-static), the experiments of tensile test after [32] are adopted and at high strain rate, the results of compressive test following [33] are chosen. Furthermore, the predicted damage data are compared with those of experiments in Fig. 5b. It is noted that there are no damage data for steel 1045 at high strain rate. These comparisons show a good agreement between simulations and experiments.
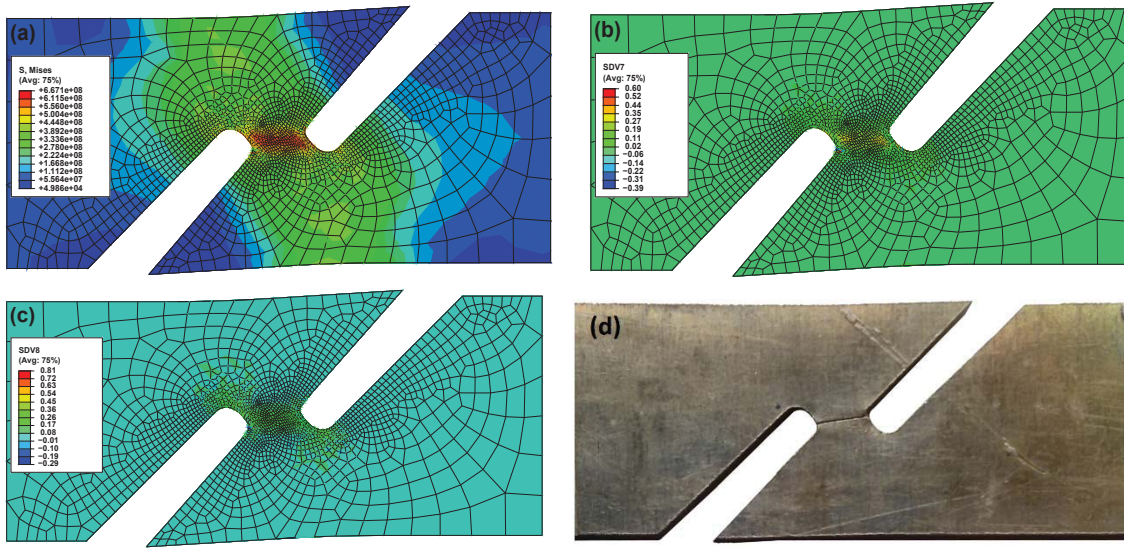


Fig. 3. Deformed shear specimen of aluminum 2024-T3. Distribution of: (a) stress (b) plastic strain (c) damage and (d) experiment.
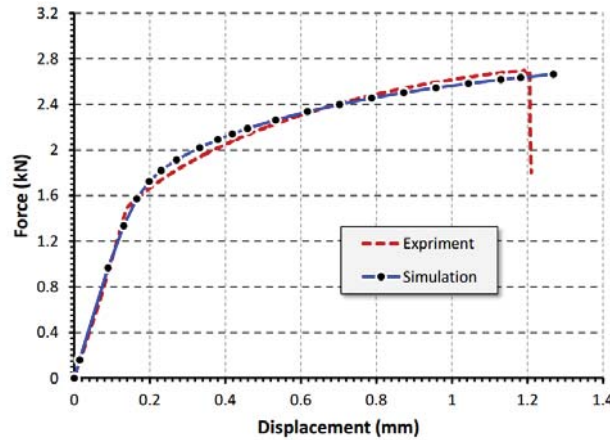


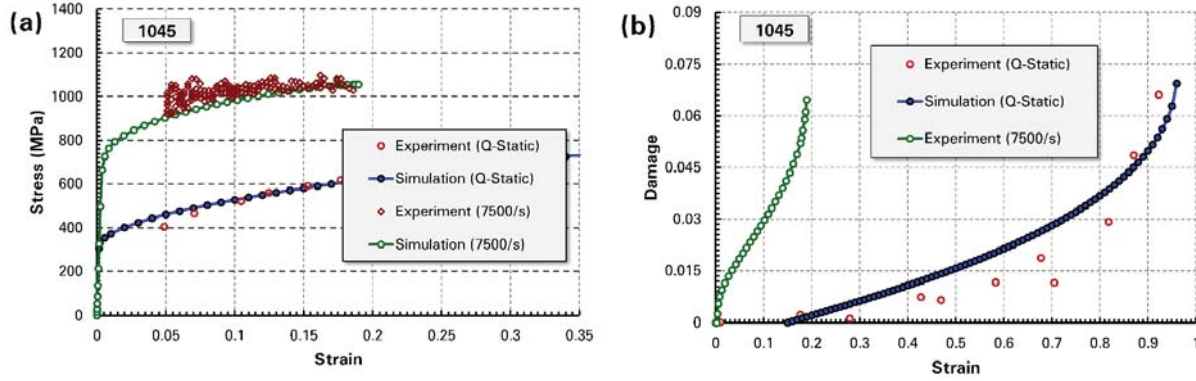Fig. 4. load-displacement curve of shear specimen.

Fig. 5. Behavior curves of steel 1045 at low [32] and high [33] strain rates: (a) stress-strain, (b) damage-strain.

The double-notched test was conducted to probe the propagation of crack path. The double-notched specimen with its dimensions are shown in Fig. 6 with the thickness of 3.2 mm. The specimen was stretched with two different stain-rates, and subsequently, load and displacement history for subsequent analysis were recorded.
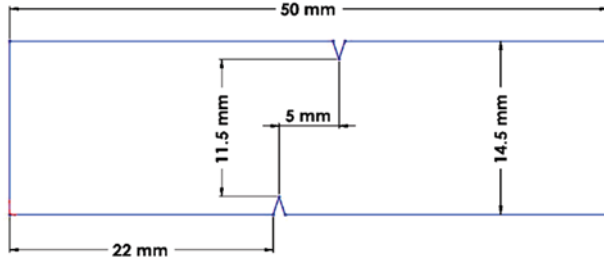


Fig. 6. Geometry and dimension of double-notched specimen (mm) with 3.2 mm thickness.

In order to capture the growth of damage in simulation, we need to enable the element deletion flag which can only be used in the explicit simulation. Therefore, the double-notched test is simulated by implementing the proposed constitutive model in the finite element program ABAQUS/Explicit via a user's material subroutine coded as VUMAT. Two types of mesh refinements, coarse and fine, are used, shown in Fig. 7.

The crack propagation path for these different mesh refinements are shown in Fig. 8a and Fig. 8b while the fractured specimen is plotted in Fig. 8c. According to the results shown in Fig. 8, the path of crack growth is suitably predicted by two mesh refinement schemes. Furthermore, the load-

displacement curve of the specimen is shown in Fig. 9. Although there is a slight deviation between the load-displacement curves with respect to two levels of mesh refinement, the predicted numerical results are in good agreement with those obtained experimentally.
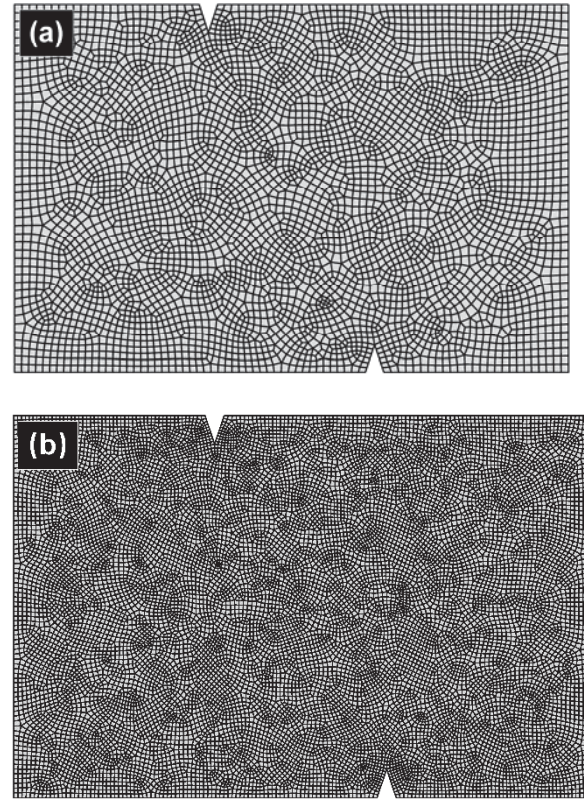


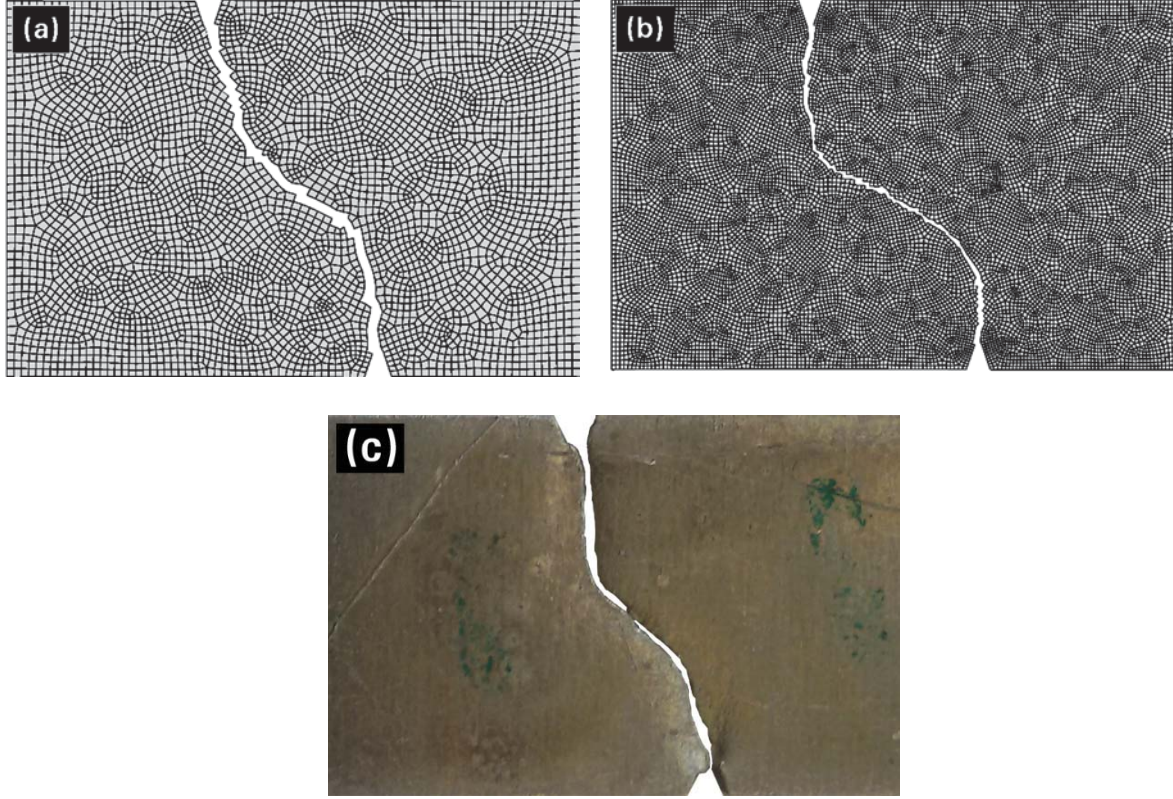Fig. 7. Two mesh refinement types of the double-notched specimen: (a) coarse, (b) fine.

Fig. 8. Crack path in deformed double-notched specimen of Al2024-T3: (a) coarse mesh, (b) fine mesh, (c) experiment
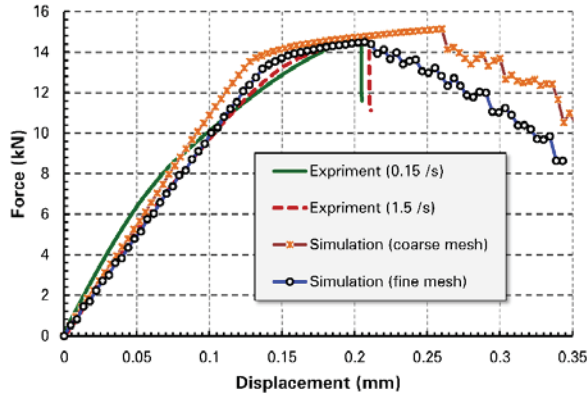


Fig. 9. Load-displacement curve in double-notched test.

## 5. Conclusions

In this paper, a rate-dependent damage model has been presented in the framework of Continuum Damage Mechanics and *Consistency* approach. The model has been presented based on the irreversible thermodynamics with internal variables. In this regard, two plastic and damage surfaces have been defined to distinguish the plastic deformation and the damage growth. The plastic yield surface is presented in the category of *Consistency*–type model in which the rate of state variables is considered as independent state variables. The proposed constitutive equations have been integrated using *generalized trapezoidal* algorithm. The algorithm has been employed for simulating the static/dynamic loadings via the implementation of the model as a user-defined subroutine UMAT/VUMAT in the ABAQUS finite element program. In order to validate the model, the predicted curves of stress-strain and damage-strain for some materials are compared with those of experiments. Furthermore, the simulation of the shear test, statically, and double-notched test, dynamically, are compared with experimental results. The excellent agreement between the data exhibits the verification of the model.

**References:**

[1]  J. A. Zukas, 1990, *High velocity impact dynamics*, John Wiley, New York

[2]  T. Børvik, O. Hopperstad, T. Berstad, M. Langseth, A computational model of viscoplasticity and ductile damage for impact and penetration, *European Journal of Mechanics-A/Solids,* Vol. 20, No. 5, pp. 685-712, 2001.

[3]  L. L. Wang, F. H. Zhou, Z. J. Sun, Y. Z. Wang, S. Q. Shi, Studies on rate-dependent macro-damage evolution of materials at high strain rates, *International Journal Of Damage Mechanics*, 2010.

[4]  J. DiLellio, W. Olmstead, Numerical solution of shear localization in Johnson-Cook materials, *Mechanics of Materials,* Vol. 35, No. 3-6, pp. 571-580, 2003.

[5]  R. Mahnken, M. Johansson, K. Runesson, Parameter estimation for a viscoplastic damage model using a gradient-based optimization algorithm, *Engineering Computations,* Vol. 15, No. 7, pp. 925-955, 1998.

[6]  M. Johansson, R. Mahnken, K. Runesson, Efficient integration technique for generalized viscoplasticity coupled to damage, *International Journal for Numerical Methods in Engineering,* Vol. 44, No. 11, pp. 1727-1747, 1999.

[7]  P. Perzyna, Fundamental problems in viscoplasticity, *Advances in Applied Mechanics,* Vol. 9, pp. 243-377, 1966.

[8]  G. Duvaut, J. L. Lions, 1972, *Les inéquations en mécanique et en physique*, Dunod, Paris

[9]  J. P. Ponthot, Radial return extensions for visco-plasticity and lubricated friction, in *Proceeding of*.

[10] W. M. Wang, 1997, *Stationary and propagative instabilities in metals: a computational point of view*, Delft University Press,

[11] W. M. Wang, L. J. Sluys, R. De Borst, Viscoplasticity for instabilities due to strain softening and strain-rate softening, *International Journal for Numerical Methods in Engineering,* Vol. 40, No. 20, pp. 3839-3864, 1997.

[12] O. M. Heeres, A. S. J. Suiker, R. de Borst, A comparison between the Perzyna viscoplastic model and the Consistency viscoplastic model, *European Journal of Mechanics-A/Solids,* Vol. 21, No. 1, pp. 1-12, 2002.

[13] M. Ristinmaa, N. S. Ottosen, Consequences of dynamic yield surface in viscoplasticity, *International Journal of Solids and Structures,* Vol. 37, No. 33, pp. 4601-4622, 2000.

[14] T. Saksala, D. Brancherie, I. Harari, A. Ibrahimbegovic, Combined continuum damage-embedded discontinuity model for explicit dynamic fracture analyses of quasi-brittle materials, *International Journal for Numerical Methods in Engineering,* Vol. 101, No. 3, pp. 230-250, 2015.

[15] R. Zaera, J. Fernández-Sáez, An implicit consistent algorithm for the integration of thermoviscoplastic constitutive equations in adiabatic conditions and finite deformations, *International Journal of Solids and Structures,* Vol. 43, No. 6, pp. 1594-1612, 2006.

[16] K. Hashiguchi, T. Okayasu, K. Saitoh, Rate-dependent inelastic constitutive equation: the extension of elastoplasticity, *International Journal of Plasticity,* Vol. 21, No. 3, pp. 463-491, 2005.

[17] J. C. Simo, J. W. Ju, Strain- and stress-based continuum damage models - I. Formulation, *International Journal of Solids and Structures,* Vol. 23, pp. 821-840, 1987.

[18] M. Johansson, K. Runesson, Viscoplasticity with dynamic yield surface coupled to damage, *Computational Mechanics,* Vol. 20, No. 1, pp. 53-59, 1997.

[19] C. L. Chow, X. J. Yang, E. Chu, Viscoplastic constitutive modeling of anisotropic damage under nonproportional loading, *Journal of Engineering Materials and Technology,* Vol. 123, No. 4, pp. 403-408, 2001.

[20] X. Ren, J. Li, A unified dynamic model for concrete considering viscoplasticity and rate-dependent damage, *International Journal of Damage Mechanics,* Vol. 22, No. 4, pp. 530-555, 2013.

[21] T. Carniel, P. Muñoz-Rojas, M. Vaz, A viscoelastic viscoplastic constitutive model including mechanical degradation: Uniaxial transient finite element formulation at finite strains and application to space truss structures, *Applied Mathematical Modelling,* Vol. 39, No. 5, pp. 1725-1739, 2015.

[22] R. K. A. Al-Rub, A. H. Tehrani, M. K. Darabi, Application of a large deformation nonlinear-viscoelastic viscoplastic viscodamage constitutive model to polymers and their composites, *International Journal of Damage Mechanics,* Vol. 24, No. 2, pp. 198-244, 2015.

[23] G. Z. Voyiadjis, F. H. Abed, A coupled temperature and strain rate dependent yield function for dynamic deformations of bcc metals, *International Journal of Plasticity,* Vol. 22, No. 8, pp. 1398-1431, 2006.

[24] C. L. Chow, J. Wang, Ductile fracture characterization with an anisotropic continuum damage theory, *Engineering Fracture Mechanics,* Vol. 30, No. 5, pp. 547-563, 1988.

[25] C. Chow, T. Lu, On evolution laws of anisotropic damage, *Engineering Fracture Mechanics,* Vol. 34, No. 3, pp. 679-701, 1989.

[26] A. Rusinek, J. A. Rodríguez-Martínez, A. Arias, A thermo-viscoplastic constitutive model for FCC metals with application to OFHC copper, *International Journal of Mechanical Sciences,* Vol. 52, No. 2, pp. 120-135, 2//, 2010.

[27]   G. Z. Voyiadjis, F. H. Abed, Microstructural based models for bcc and fcc metals with temperature and strain rate dependency, *Mechanics of Materials,* Vol. 37, No. 2–3, pp. 355-378, 2//, 2005.

[28]   R. Liang, A. S. Khan, A critical review of experimental results and constitutive models for BCC and FCC metals over a wide range of strain rates and temperatures, *International Journal of Plasticity,* Vol. 15, No. 9, pp. 963-980, //, 1999.

[29]   C. L. Chow, J. Wang, An anisotropic theory of continuum damage mechanics for ductile fracture, *Engineering Fracture Mechanics,* Vol. 27, No. 5, pp. 547-558, 1987.

[30]   M. Ganjiani, Identification of damage parameters and plastic properties of an anisotropic damage model by micro-hardness measurements, *International Journal of Damage Mechanics*, March 27, 2013, 2013.

[31]   A. Mkaddem, F. Gassara, R. Hambli, A new procedure using the microhardness technique for sheet material damage characterisation, *Journal of Materials Processing Technology,* Vol. 178, No. 1-3, pp. 111-118, 2006.

[32]   G. Le Roy, J. D. Embury, G. Edward, M. F. Ashby, A model of ductile fracture based on the nucleation and growth of voids, *Acta Metallurgica,* Vol. 29, pp. 1509-1522, 1981.

[33]   S. P. F. C. Jaspers, J. H. Dautzenberg, Material behaviour in conditions similar to metal cutting: flow stress in the primary shear zone, *Journal of Materials Processing Technology,* Vol. 122, pp. 322-330, 2002.